Path-integral Monte-Carlo simulations for electronic dynamics on molecular chains: I. Sequential hopping and super exchange

Lothar Mühlbacher,* Joachim Ankerhold, and Charlotte Escher

Physikalisches Institut, Albert-Ludwigs-Universität, D-79104 Freiburg, Germany

(Dated: Date: November 21, 2018)

An improved real-time quantum Monte Carlo procedure is presented and applied to describe the electronic transfer dynamics along molecular chains. The model consists of discrete electronic sites coupled to a thermal environment which is integrated out exactly within the path integral formulation. The approach is numerically exact and its results reduce to known analytical findings (Marcus theory, golden rule) in proper limits. Special attention is paid to the role of superexchange and sequential hopping at lower temperatures in symmetric donor-bridge-acceptor systems. In contrast to previous approximate studies, superexchange turns out to play a significant role only for extremely high lying bridges where the transfer is basically frozen or for extremely low temperatures where for weaker dissipation a description in terms of rate constants is no longer feasible. For bridges with increasing length an algebraic decrease of the yield is found for short as well as for longer bridges. The approach can be extended to electronic systems with more complicated topologies including impurities and in presence of external time dependent forces.

I. INTRODUCTION

Electron transfer (ET) processes are one of the fundamental phenomena in complex molecular systems [1], the most prominent one being the primary step of photosynthesis [2, 3]. In the last decade or so much theoretical and experimental efforts have been focused on bridged molecular systems where the transfer from a donor to an acceptor is mediated by a molecular structure connecting them [4, 5, 6, 7, 8, 9]. Particular attention has been paid to DNA complexes with to some extent still controversial results [10]. Of foremost importance are donor-bridge-acceptor (DBA) systems in the strongly rising field of molecular electronics [11, 12, 13, 14, 15]. Based on advanced methods of synthetic chemistry, nowadays, bridge units with specific chemical and physical properties can be produced and linked to donor/acceptor species or contacted with metal leads and thus integrated into electrical circuits.

Since the pioneering work of Marcus and Jortner [1, 2, 3] the influence of residual vibronic modes and a solvent environment on the ET is known to be extremely crucial. In fact, the presence of a dissipative surrounding is the prerequisite for a directed (irreversible) transport across DBA complexes meaning that bath parameters such as temperature and spectral densities have a sensitive impact [16, 17]. Accordingly, basically two distinct transport channels have been identified. For high lying and short bridges quantum mechanical tunneling gives rise to a superexchange mechanism associated with a characteristic exponentially decreasing yield with increasing bridge length. If the bridge is sufficiently long, however, sequential transfer processes (hopping) dominate based on thermal activation. Theoretically the competition between these channels has been investigated

based on Redfield theory and simple system+reservoir models in Ref. [4] and more recently in Refs. [5, 6, 8]. In these studies the mentioned exponential length dependence as well as an algebraic decrease of the transfer rate in case of a sequential mechanism has been found empirically. This latter behavior has been also derived explicitly from a more rigorous formulation in Ref. [9]. In most of these previous studies symmetric DBA systems were considered with degenerate donor/acceptor and degenerate bridge states since they already display the essential features and make the analysis particularly transparent. Additional simplifying assumptions about the nature of the thermal bath coupled to the ET have been invoked to obtain explicit results since, as for most dissipative quantum systems [18], a numerical description is extremely demanding.

Indeed, it has been one of the major challenges in recent years in physics and chemistry to develop efficient algorithms to get access to a detailed analysis of these systems. As shown first by Feynman and Vernon [19] and in the 1980s by Caldeira and Leggett [20], the path integral representation is particularly suited as a starting point. Namely, for Gaussian bath fluctuations the environmental degrees of freedom can be eliminated exactly leading to the reduced system dynamics. In contrast to perturbative approaches as e.g. Redfield theory this formulation has the merit of being applicable down to zero temperature, to adiabatic bath modes, and strong friction. A direct numerical evaluation of the corresponding path integral expression for the density matrix is not possible though. The reason for that are the interactions, non-local in time, among forward and backward paths generated by the bath degrees of freedom. Typically, the range of these interactions grows with $\hbar\beta$. An efficient numerical approach that relies on a finite interaction range for sufficiently high temperatures has been developed by Makri and co-workers [21] and applied to a variety of systems meanwhile.

Presently, the only numerically exact approach is given

by path integral Monte Carlo (PIMC) simulations [22]. It has been successfully applied to the spin-boson system to study e.g. the influence of nonequilibrium initial bath distributions [23], the role of vibronic and electronic coherences [23, 24], and electronic transfer rates in large ranges of parameter space [25]. For a DBA system with one intermediate electronic site (three-state system) which can be seen as simple model for the primary charge separation of photosynthesis PIMC results could describe most of the experimental key features [26]. One fundamental problem of the PIMC, though, is intimately connected with the constitutive role of interferences in quantum mechanical systems. Known as the *dynamical sign problem* [22], it turns out that the number of sample paths needed to achieve a sufficient signal-to-noise ratio increases exponentially with the simulated system time. To partially circumvent this drawback various techniques have been introduced and shown to stabilize the simulations considerably [26, 27, 28, 29, 31].

The goal of this paper is twofold: On the one hand the challenge is to present a PIMC approach applicable to larger discrete systems and longer simulation times in order to lay the basis to treat bridge systems with more electronic sites, a complicated topology including impurities, and/or in presence of external periodic driving. On the other hand, motivated by the above mentioned works on symmetric bridges, our intention is to investigate the role of the superexchange and the sequential mechanisms in ET within a complete system+reservoir model and with a numerically exact approach. This way, we avoid simplifying assumptions about the bath, the system-bath coupling, or the structure of the bath along the molecular bridge. Accordingly, our results can directly be compared with analytical rate expressions derived within Marcus theory [18], golden rule approaches [32], or cluster expansion methods [33]. Surprisingly, such an analysis of numerical results within the context of the available theoretical findings is still missing.

The paper is organized as follows: We start in Sec. II by defining the system and the bath and introducing its path integral representation. In Sec. III the connection to the description in terms of Master equations is revealed and known results for the electronic transfer rates are discussed. Then, in Sec. IV the PIMC used and developed in this paper is presented, which leads to a substantial improvement in efficiency compared to previous PIMC schemes. Only this allows us to study in Sec. V first the three-state system and then complexes with longer bridges in detail, particularly with very good signal to noise ratio and larger times. A Conclusion contains our main results and some remarks about subsequent work.
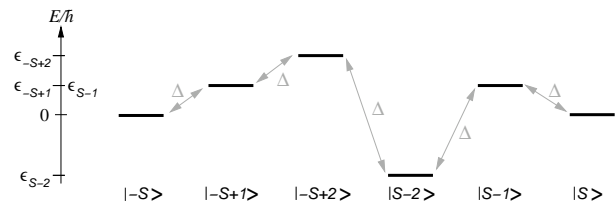

FIG. 1: Molecular chain for $S = 2\,^1/_2$ ($d = 6$) and constant nearest neighbor coupling Δ.

II. THEORY

A. Dynamics of the dissipative d-level system

We investigate the dynamics of a single electron moving on a chain of $d = 2S + 1$ discrete sites, labeled by a discrete variable $-S \leq s \leq S$ with spacing 1, separated by equal distances a but arbitrary energies $\hbar\epsilon_s$ (see Fig. 1). Electronic motion is facilitated through tunneling between sites s and s', with a real tunneling amplitude $\Delta_{s,s'}$. The electronic coordinate can then be expressed as

$$q(t) = a \cdot s(t) \,, \tag{1}$$

where $-S \leq s(t) \leq S$. The position operator thus is equivalent to the spin S operator

$$a\mathbf{S}_z|s\rangle = as|s\rangle \,, \tag{2}$$

with $|s\rangle$ denoting the (orthonormal) localized electronic states. In terms of electron transfer, $|-S\rangle$ and $|S\rangle$ represent the donor and acceptor, respectively, while the other states are referred to as the bridge states.

The free d-level system (dLS) Hamiltonian can then be written as

$$H_{d\mathrm{LS}} = \hbar\mathbf{E}_z - \hbar\mathbf{S}_x \,, \tag{3}$$

where $\mathbf{E}_z$ describes the energetic distribution of the electronic sites according to

$$\mathbf{E}_z|s\rangle = \epsilon_s|s\rangle \,, \tag{4}$$

while $\mathbf{S}_x$ governs the tunneling,

$$\mathbf{S}_x = \sum_{s<s'=-S}^{S} \Delta_{s,s'} \left(|s\rangle\langle s'| + |s'\rangle\langle s| \right) \,. \tag{5}$$

Of particular importance is the case of nearest neighbor tunneling only with

$$\begin{aligned} \mathbf{S}_x|s\rangle &= \Delta_{s-1,s}|s-1\rangle + \Delta_{s,s+1}|s+1\rangle \\ &\quad \text{for } -S < s < S \,, \\ \mathbf{S}_x|-S\rangle &= \Delta_{-S,-S+1}|-S+1\rangle \,, \\ \mathbf{S}_x|S\rangle &= \Delta_{S,S+1}|S-1\rangle \,. \end{aligned} \tag{6}$$

We already note here that the propagation of the free d-level system is most conveniently performed not in the

site representation used above, but rather in the eigenstate representation of $H_{d\text{LS}}$ (for details see Sec. IV). This is completely equivalent to the transformation between (localized) Wannier states and delocalized molecular orbitals (Bloch states) in infinite tight binding lattices. The site representation is particularly suited, however, to include the interaction with solvent and vibronic degrees of freedom which later on will be integrated out. For this purpose, we embed the $d\text{LS}$ in a system-plus-reservoir model, leading to the total Hamiltonian [18]

$$
\begin{aligned}
H &= H_{d\text{LS}} + H_I + H_B \\
&= H_{d\text{LS}} - a\mathbf{S}_z \sum_\alpha c_\alpha X_\alpha + (a\mathbf{S}_z)^2 \sum_\alpha \frac{c_\alpha^2}{2m_\alpha \omega_\alpha^2} \\
&\quad + \sum_\alpha \left(\frac{P_\alpha^2}{2m_\alpha} + \frac{1}{2} m_\alpha \omega_\alpha^2 X_\alpha^2 \right) .
\end{aligned}
\tag{7}
$$

The residual degrees of freedom are thus modeled by an infinite collection of harmonic oscillators, H_B, which bilinearly couple to the position of the electron (H_I). The so-called counterterm quadratic in the $d\text{LS}$ position operator $a\mathbf{S}_z$, which reduces to a physically irrelevant constant for $S = 1/2$, prevents a renormalization of the electronic energy levels by the oscillator bath [18]. As discussed in detail in Refs. [16, 17, 18, 32] this provides a reasonably accurate description of reality for the great majority of ET systems. It turns out that for the electronic dynamics the environmental parameters enter via the spectral density

$$
J(\omega) = \frac{\pi a^2}{2\hbar} \sum_\alpha \frac{c_\alpha^2}{m_\alpha \omega_\alpha} \delta(\omega - \omega_\alpha) ,
\tag{8}
$$

which effectively becomes a continuous function of ω for a condensed-phase environment. The Gaussian statistics of the environment is determined by the complex-valued bath autocorrelation function which for real time t reads

$$
\begin{aligned}
L(t) &= \frac{1}{\hbar^2} \left\langle \left(\sum_\alpha c_\alpha X_\alpha(t) \right) \left(\sum_\alpha c_\alpha X_\alpha(0) \right) \right\rangle_\beta \\
&= \frac{1}{\pi} \int_0^\infty d\omega \, J(\omega) \frac{\cosh[\omega(\hbar\beta/2 - it)]}{\sinh(\hbar\beta\omega/2)} ,
\end{aligned}
\tag{9}
$$

where $\beta = 1/k_B T$. For $S = 1/2$, Eq. (7) represents the celebrated *spin-boson* (SB) model, with numerous applications in solid-state physics [18]. In the special case of a constant nearest coupling, i.e. $\Delta_{s,s'} = \delta_{s'-s,1}\Delta$ for all s, s', the described compound reduces to a generalization of the SB model, as it in fact then resembles a "spin-S-boson model" [18]. In the following, we repeatedly will take advantage of the striking similarity. To make connection to (classical) two-state ET theory, we also mention the classical *reorganization energy* $\hbar\Lambda_{\text{cl}}$ of the Marcus theory [2, 3],

$$
\Lambda_{\text{cl}} = \frac{1}{\pi} \int_0^\infty d\omega \, \frac{J(\omega)}{\omega} .
\tag{10}
$$

For the dissipative electronic dynamics we focus on the *time-dependent site populations*,

$$
P_{s_f, s_i}(t) = \text{Tr} \left\{ e^{iHt/\hbar} |s_f\rangle\langle s_f| e^{-iHt/\hbar} W_i(0) \right\} ,
\tag{11}
$$

which are normalized, $\sum_{s_f=-S}^{S} P_{s_f, s_i}(t) = 1$, and where $W_i(0)$ specifies the initial state of the total compound. In most theoretical and experimental works an initial separation of the electron and the environment is assumed corresponding to an initial density matrix

$$
W_i(0) = Z_B^{-1} |s_i\rangle\langle s_i| e^{-\beta(H_B - s_i \mu\mathcal{E})} ,
\tag{12}
$$

with the electron held fixed in state $|s_i\rangle$ and the bath normalization $Z_B = \text{Tr}\{e^{-\beta H_B}\}$ assuring the full system's density matrix to be normalized for all times. For a transfer process across the entire chain one typically prepares the electron initially in the donor state, i.e. $|s_i\rangle = |-S\rangle$ [4, 8]. Above, μ is the dipole moment of the electron, and $\mathcal{E}$ denotes the dynamical polarization of the bath [18], which is equilibrated with respect to the initial position of the electron. By comparing with Eq. (7), we see that $\mu\mathcal{E} = a \sum_\alpha c_\alpha X_\alpha$. As pointed out in Ref. [25], this "standard preparation" often used in ET experiments is especially suitable for a theoretical description of thermal transfer rates.

The present formulation can easily be extended in order to describe the impact of an external time dependent driving force. This as well as abandoning the restriction to nearest neighbor coupling will be the subject of a subsequent paper.

B. Path integral representation

The path integral representation provides a formally exact expression for the dynamics of the electronic population and is thus the starting point for a numerically exact Monte-Carlo (MC) scheme. The standard procedure is then to eliminate the bath degrees of freedom to arrive at the reduced dynamics. This can be done exactly due to the harmonic nature of the bath. As shown in Ref. [18], one thus obtains for Eq. (11)

$$
P_{s_f, s_i}(t) = \frac{1}{Z} \oint \mathcal{D}\tilde{s} \, \delta_{\tilde{s}(t), s_f} \exp\left\{ \frac{i}{\hbar} S_{d\text{LS}}[\tilde{s}] - \Phi[\tilde{s}] \right\} .
\tag{13}
$$

Here the path integration runs over closed paths $\tilde{s}(\tilde{t})$ starting at $\tilde{s}(0) = s_i$ and propagating along the real-time contour $\tilde{t} \in 0 \to t \to 0$, which connect the forward and backward paths $s(t')$ and $s'(t')$, respectively. Furthermore, $S_{d\text{LS}}[s]$ denotes the total action of the free $d\text{LS}$, and the influence of the traced-out bath is encoded in the *Feynman-Vernon influence functional* $\Phi[s]$ [19]. In terms of the bath autocorrelation function (9), it reads [18]

$$
\Phi[s, s'] = \int_0^t dt' \int_0^{t'} dt'' [s(t') - s'(t')] \, [L(t'-t'')s(t'')
$$

$$- L^*(t' - t'')s'(t'')]$$

$$+ i\frac{\hat{\mu}}{2} \int_0^t dt'[s^2(t') - s'^2(t')] , \qquad (14)$$

where

$$\hat{\mu} = \frac{2}{\pi} \int_0^\infty d\omega \frac{J(\omega)}{\omega} = 2\Lambda_{\rm cl} . \qquad (15)$$

The influence functional introduces long-ranged nonlocal interactions among the dLS paths so that in general an explicit evaluation of the remaining path integral in Eq. (13) is possible only numerically. Before we explain the details of the PIMC scheme in Sec. IV, however, we focus in the next Section on the description of the population dynamics in terms of Master equations with associated transition rates. Corresponding results will provide the appropriate tools in order to analyze and understand the MC data.

III. POPULATION DYNAMICS

A. Master equations

As has been derived in Ref. [33], the dynamics of the population for a spin-S-boson system can be cast exactly into the form of a retarded non-local (in time) Master equation

$$\frac{dP_{s_f,s_i}(t)}{dt} = \sum_{s=-S}^{S} \int_0^t dt' \, \tilde{\Gamma}_{s,s_i}(t - t') \, P_{s,s_i}(t') \qquad (16)$$

with time dependent transition rates $\tilde{\Gamma}_{s,s_k}(t)$ the Laplace transforms of which are given by appropriate cluster functions. Provided the dissipative influence is sufficiently strong or temperature sufficiently high, the electronic dynamics (16) can be simplified to a conventional Master equation. In essence, one invokes a coarse graining procedure in time so that after some initial transient motion, i.e. for $t > \tau_{\rm trans}$, the population dynamics obeys

$$\dot{P}_{s_f,s_i}(t) = \sum_{s=-S}^{S} \Gamma_{s,s_i} \, P_{s,s_i}(t) . \qquad (17)$$

Here, the nearest neighbor transition rates $\Gamma_{s,s\pm1}$ are related to sequential hopping processes, while $\Gamma_{-S,S}$ describes direct transfer from donor to acceptor without any real populations in the bridge states (superexchange).

In the case studied here in more detail, namely, degenerate donor and acceptor energies ($\epsilon_{-S} = \epsilon_S = 0$), degenerate bridge energies ($\epsilon_{-S+1} = \ldots = \epsilon_{S-1} = \epsilon$), and nearest neighbor tunneling with $\Delta_{s,s'} = \delta_{s'-s,1}\Delta$, the number of independent rates shrinks considerably. Eq. (17) becomes particularly simple in case of purely sequential transport where it can be written as

$$\dot{\mathbf{P}} = A\mathbf{P} , \qquad (18)$$

with the rate matrix

$$A = \begin{pmatrix} -\Gamma_{DB} & \Gamma_{BD} & 0 & & \cdots & & 0 \\ \Gamma_{DB} & -(\Gamma_{BD}+\Gamma_B) & \Gamma_B & 0 & & \cdots & \\ 0 & \Gamma_B & -2\Gamma_B & \Gamma_B & & 0 & \\ \vdots & & \ddots & \ddots & \ddots & & \vdots \\ & 0 & \Gamma_B & -2\Gamma_B & \Gamma_B & 0 \\ & \cdots & & 0 & \Gamma_B & -(\Gamma_B+\Gamma_{BA}) & \Gamma_{AB} \\ 0 & & \cdots & & 0 & \Gamma_{BA} & -\Gamma_{AB} \end{pmatrix} \qquad (19)$$

Here, $\mathbf{P} = (P_D, P_{B1}, \ldots, P_{Bb}, P_A)$ where P_D (P_A) refers to the donor (acceptor) population P_{-S} (P_S) and P_{Bi} to the population P_{i-S} of the $b = d - 2$ bridge states. The rate constants Γ_{DB} (Γ_{BD}) govern the sequential forward (backward) transport between donor and first bridge state, Γ_{AB} (Γ_{AD}) the sequential forward (backward) transport between acceptor and last bridge state, and Γ_B the sequential transport on the bridge. Coherent transport (superexchange) would be accounted for by additional rate contributions in the upper and lower triangular of A.

According to Eq. (18) the populations $P_s(t)$ re-

flect multi-exponential dynamics, with the corresponding rates given by the eigenvalues of the rate matrix A. The approach to equilibrium happens to be on the relaxation time scale τ_R which is the inverse of the smallest of these eigenvalues Γ_R. Forward and backward rates in A are connected via detailed balance,

$$\Gamma_{BD} = \frac{P_B^\infty}{P_D^\infty}\Gamma_{DB} = \frac{2P_B^\infty}{1 - bP_B^\infty}\Gamma_{DB} , \qquad (20)$$

where P_B^∞ and P_D^∞ denote the equilibrium occupation probabilities of the bridge states and the donor, while for symmetry reasons $P_A^\infty = P_D^\infty$, $\Gamma_{BA} = \Gamma_{BD}$, and

$\Gamma_{AB} = \Gamma_{DB}$. The equilibrium occupation probabilities are Boltzmann distributed with respect to an effective electronic parameter $\tilde{\epsilon}(\beta)$ which, for strong damping and/or higher temperatures, converges with the physical bias ϵ [34]. It is then straightforward to calculate $P_s(t)$ from Eq. (18) or the more general expression (17) which in the appropriate parameter range gives an accurate description of the exact dynamics for times t larger than some transient time scale t_{trans}. The corresponding expressions for $d = 3$ are given in App. B.

Hence, once MC data for the populations are generated, the associated rate constants are obtained by fitting the electronic dynamics obtained from Eqs. (18) and (19) to the numerical data. At sufficiently low temperatures, however, coherent oscillations govern the population dynamics over a long period of time and the transfer can no longer be characterized by time independent decay rates. Outside this range information about the impact of superexchange can be extracted by comparing fits to the sequential (18) and the complete model (17).

B. Sequential and superexchange rate expressions

As already noted, basically two transport channels have been found in previous studies on bridge mediated ET, namely, a sequential channel and a superexchange channel. The latter one is expected to dominate for high lying and sufficiently short bridges, whereas in other cases the former one prevails. Here we briefly collect available analytical results for the transitions rates, particularly for symmetric DBA systems (degenerate donor and acceptor energies, degenerate bridge states), to analyze our PIMC results accordingly (see Sec. V).

In the classical limit $\hbar\beta\omega_c \ll 1$ the sequential forward rate is given by the well known Marcus result [3]

$$\Gamma_{DB,\mathrm{Marcus}} = \frac{\Delta^2}{1 + \pi\Delta^2/(\Lambda_{\mathrm{cl}}\omega_c)} \sqrt{\frac{\pi\hbar}{\Lambda_{\mathrm{cl}}k_B T}} \; e^{-\beta F^*(\epsilon)}$$

(21)

with the activation free energy barrier $F^*(\epsilon) = \hbar(\epsilon + \Lambda_{\mathrm{cl}})^2/(4\Lambda_{\mathrm{cl}})$ where $\epsilon = \epsilon_B - \epsilon_A$ is the energy gap between bridge and donor (acceptor). As long as a rate description is valid at all, this expression is applicable from the weak adiabatic domain ($\omega_c < \Delta$), where it eventually becomes independent of Δ, to the nonadiabatic range ($\omega_c \gg \Delta$). Recently, for adiabatic to moderate nonadiabatic environments an extension of this rate expression to lower temperatures where quantum fluctuations and nuclear tunneling come into play has been derived in Ref. [35].

In the quantum domain $\hbar\beta\omega_c \gtrsim 1$ and for small tunneling amplitudes $\Delta \ll \omega_c$ (nonadiabatic range) transfer rates are calculated perturbatively by invoking Fermi's golden rule. For the sequential forward rate the result is [18, 32]

$$\Gamma_{DB,\mathrm{GR}}(\epsilon) = \Delta^2 \int_{-\infty}^{\infty} dt \exp[-i\epsilon t - Q(t)]$$

(22)

with the damping kernel $Q(t)$ specified in Eq. (34). The golden rule rate expression reduces for high temperatures to the nonadiabatic limit of the Marcus formula (21) and captures nuclear tunneling at low T. Within a perturbative treatment in powers of Δ^{2n}, superexchange rates appear as higher order contributions $n = 2, 3, 4, \ldots$. In case of a three-state system with $\epsilon_D = \epsilon_A$, $\Gamma_{-1,1}$ is obtained in leading order $n = 2$ as [33]

$$
\begin{aligned}
\Gamma_{S,\mathrm{GR}} = 2\Delta^4 \mathrm{Re}\Bigg\{ & \int_0^\infty d\tau_1 d\tau_2 d\tau_3 \; \exp[Q^*(\tau_3) \\
& - Q(\tau_2 + \tau_3) - Q(\tau_1 + \tau_2 + \tau_3) - Q(\tau_2) \\
& - Q(\tau_1 + \tau_2) + Q(\tau_1)] \\
& \times \exp[-i\epsilon(\tau_1 - \tau_3)] \Bigg\} ,
\end{aligned}
$$

(23)

Even for this more involved expression simplifications arise in certain limits. In the high temperature range $\hbar\beta\omega_c \ll 1$, where $Q(\tau)$ can be expanded for short times, one obtains the classical superexchange rate [33]

$$
\begin{aligned}
\Gamma_{SCL,\mathrm{GR}} = & \frac{\Delta^4}{2(\epsilon - \Lambda_{\mathrm{cl}})^2} \sqrt{\frac{\pi\hbar\beta}{\Lambda_{\mathrm{cl}}}} \\
& \times \left\{ e^{-\beta\hbar\Lambda_{\mathrm{cl}}} - \frac{1}{2} \left[e^{-\beta F_+} + e^{-\beta F_-} \right] \right\}
\end{aligned}
$$

(24)

with the activation energies $F_+ = \hbar(\epsilon + \Lambda_{\mathrm{cl}})^2/4\Lambda_{\mathrm{cl}}$ and $F_- = \hbar(\epsilon - 3\Lambda_{\mathrm{cl}})^2/4\Lambda_{\mathrm{cl}}$. This rate is well-defined even in the resonant case $\epsilon \to \Lambda_{\mathrm{cl}}$ where, however, also the incoherent transfer is extremely efficient with a strong bridge population.

In presence of a quantum bath $\hbar\beta\omega_c \gtrsim 1$ the classical reorganization energy drops out of the golden rule rate, see Eq. (24), since nuclear tunneling is relevant. The superexchange expression can be simplified for a high-lying intermediate state where the DBA system can effectively be treated as an AD system with effective coupling [33], i.e.,

$$\Gamma_{SQM,\mathrm{GR}} \approx \frac{\Delta^4}{\epsilon^2} \int_{-\infty}^{\infty} d\tau \exp[-4Q(\tau)] .$$

(25)

IV. SIMULATION METHOD

As already addressed, the time evolution of a dissipative quantum system can in general not be evaluated analytically. In the past the PIMC method has been proven as a very promising approach to obtain numerically exact results even in regions of parameter space where other approximative methods fail. In particular, in recent experiments on molecular wires contacted with metal junctions [36] low temperature measurements down to 30K have been performed which necessitates the inclusion of strong quantum effects also in the environment.

For this purpose we turn to the path integral representation (13) and employ a discretization described in

detail in Refs. [25, 26]. For the forward and backward paths the time axis is sliced via q uniformly spaced points with discretization steps $\tau = t/q$. The path integral in Eq. (13) then becomes

$$P_{s_f, s_i}(t) = \sum_{\{s_j\}} \delta_{s_{q+1}, s_f} \rho[\{s_j\}] \qquad (26)$$

with

$$\rho[\{s_j\}] = \left[\prod_{k=1}^{2q} K(s_k, s_{k+1}) \right] e^{-\Phi[\{s_j\}]} . \qquad (27)$$

The sum runs over all realizations of the discretized spin path $\{s_j\} = \{s_1 \equiv s_i, s_2, \ldots, s_{2q}, s_{2q+1} \equiv s_i\}$, and $K(s_j, s_{j+1})$ denotes the coordinate representation of the free dLS propagation over the time interval τ, i.e.,

$$K(s, s', \tau) = \langle s | \exp(-i\tau H_{d\text{LS}}/\hbar) | s' \rangle . \qquad (28)$$

While in principle for the dLS Hamiltonian this propagator can be obtained by exploiting the symmetric Trotter splitting $\exp(-i\tau H_{d\text{LS}}/\hbar) = \exp(-i\tau \mathbf{E}_z/2) \exp(i\tau \mathbf{S}_x) \exp(-i\tau \mathbf{E}_z/2) + O(\tau^3)$ and evaluating $\langle s_{j+1} | \exp(i\tau \mathbf{S}_x) | s_j \rangle$, a more accurate approach follows from the eigenstate representation

$$H_{d\text{LS}} |\phi_N\rangle = E_N |\phi_N\rangle , \quad N = 1, \ldots, d . \qquad (29)$$

This way, one obtains

$$K(s, s', \tau) = \sum_{N=1}^{d} \langle s | \phi_N \rangle \langle \phi_N | s' \rangle \, e^{-i\tau E_N/\hbar} , \qquad (30)$$

which can be easily computed numerically once the dLS's parameters are specified. Another advantage of this formulation is that it can be immediately applied to all quantum systems which can be mapped effectively onto a dLS, e.g. by a proper reduction of its Hilbert space.

To arrive at a discretized form of the influence functional (14), the sum and difference coordinates

$$\eta(t') \equiv s(t') + s'(t') , \qquad \xi(t) \equiv s(t') - s'(t') \qquad (31)$$

are introduced, which read $\eta(t') = \eta_j$ ($\xi(t') = \xi_j$) for $t' \in [(j-1)\tau - \tau/2, (j-1)\tau + \tau/2]$ in their discretized form. The sum paths are also considered as "quasi-classical", while the difference paths capture quantum fluctuations [18, 26]. Equation (14) finally can be written as

$$\Phi[s_i, \eta, \xi] = i \sum_{j=2}^{q} \xi_j \hat{X}_j^{(s_i)} \qquad (32)$$

$$+ \sum_{j \geq k=2}^{q} \xi_j (iX_{j-k}\eta_k + \Lambda_{j-k}\xi_k)$$

with

$$\hat{X}_j^{(s_i)} = 2s_i \operatorname{Im}\{Q((j-2)\tau) - Q((j-1)\tau)\}$$

for $2 \leq j \leq q$,
$$\Lambda_0 = \operatorname{Re}\{Q(\tau)\} ,$$
$$X_0 = \operatorname{Im}\{Q(\tau)\} ,$$
$$\Lambda_l = \operatorname{Re}\{Q((l-1)\tau) + Q((l+1)\tau) - 2Q(l\tau)\}$$
$$\text{for } 1 \leq l \leq q-2 ,$$
$$X_l = \operatorname{Im}\{Q((l-1)\tau) + Q((l+1)\tau) - 2Q(l\tau)\}$$
$$\text{for } 1 \leq l \leq q-2 . \qquad (33)$$

Here, one has introduced the twice-integrated bath autocorrelation function $Q(t)$ defined by $\ddot{Q}(t) = L(t)$, $Q(0) = 0$ with $\dot{Q}(0) = i\Lambda_{\text{cl}}$. Explicitly it is gained from Eq. (9) to read

$$Q(t) = \frac{1}{\pi} \int_0^\infty d\omega \frac{J(\omega)}{\omega^2} \{\coth(\hbar\beta\omega/2))[1 - \cos(\omega t)]$$
$$+ i\sin(\omega t)\} . \qquad (34)$$

In the sequel we consider a spectral density of the form

$$J(\omega) = 2\pi\alpha\omega e^{-\omega/\omega_c} , \qquad (35)$$

which is equivalent to ohmic damping with a cut-off frequency ω_c. In this case $Q(t)$ can be calculated analytically and one obtains

$$Q(t) = 2\alpha \left[\ln(1 + i\omega_c t) - \ln \frac{\Gamma(\Omega + it/\hbar\beta)\Gamma(\Omega - it/\hbar\beta)}{\Gamma^2(\Omega)} \right] \qquad (36)$$

with $\Omega = 1 + 1/(\hbar\beta\omega_c)$ and the Gamma function $\Gamma(z)$.

Equations (26), (27) and (32) constitute a discretized form of the populations (11) and thus provide a starting point for PIMC simulations. Unfortunately, this method is handicapped by the dynamical sign problem [22]. It originates from quantum interferences between different system paths $\{s_j\}$, causing a small signal-to-noise ratio of the stochastic averaging procedure: The exponential increase of the paths' configuration space with the maximum real time under study results in an exponential decrease of the signal-to-noise ratio. Various procedures to mitigate the sign problem have been proposed in the past, like maximum entropy methods [27], filter techniques [28, 29] or the multilevel blocking approach [25, 31]. Here we employ a filter technique optimized for dissipative spin systems as suggested by Egger and Mak [26] which exploits the special symmetries of the influence functional.

The backbone of this approach is the observation that the absence of a self-energy like term for the quasi-classical paths $\{\eta_j\}$ in Eq. (32) allows to express the summation over the latter as a series of $q - 1$ matrix multiplications. This usually requires drastically less computational effort than performing the corresponding sums in Eq. (26) and thus can be carried out explicitly. It reduces the degrees of freedom from the $2q - 1$ variables $\{\eta_{2 \leq j \leq q+1}, \xi_{2 \leq j \leq q}\}$ to the $q - 1$ quantum variables $\{\xi_{2 \leq j \leq q}\}$ and therefore significantly improves the numerical stability of the corresponding MC

simulations. Explicitly, after switching to the quasi-classical and quantum coordinates (31) and defining the $[2(S-|\xi_j|)+1] \times [2(S-|\xi_{j+1}|)+1]$ matrices $\hat{K}^{(j)}$ according to

$$\hat{K}^{(j)}_{\eta_j,\eta_{j+1}}(\xi_j,\ldots,\xi_q)$$

$$\equiv \exp\left(-i\eta_{j+1}\sum_{k>j}\xi_k X_{k-j-1}\right)$$

$$\times K((\eta_j+\xi_j)/2,(\eta_{j+1}+\xi_{j+1})/2)$$

$$\times K^*((\eta_j-\xi_j)/2,(\eta_{j+1}-\xi_{j+1})/2),\qquad (37)$$

the population (26) becomes

$$P_{s_f,s_i}(t) = \sum_{\{\xi_j\},\eta_{q+1}} \delta_{\eta_{q+1},2s_f}\exp\left[-\sum_{j=2}^{q}\xi_j\left(i\hat{X}_j^{(s_i)}\right.\right.$$

$$\left.\left.+\sum_{k\geq j}\xi_k\Lambda_{k-j}\right)\right]$$

$$\times\hat{K}^{(1)}(0,\xi_2,\ldots,\xi_q)\cdots\hat{K}^{(q)}(\xi_q). \quad (38)$$

Here, the sum over the $\{\eta_{j\leq q}\}$ has been written as a product over the q matrices $\hat{K}^{(j)}$, where the first (last) of them is only a row (column) vector due to $\eta_1 \equiv 2s_i$ ($\eta_{q+1} \equiv 2s_f$). This matrix product can be performed explicitly such that only the sum over the quantum variables $\{\xi_j\}_{2\leq j\leq q}$ has to be evaluated by PIMC simulations. The resulting mitigation of the sign problem allows for numerically stable simulations which consume significantly less CPU time than corresponding ones evaluating the standard expression (26). Moreover, another considerable speedup can be gained by optimizing the MC weight with respect to the dissipative regime (see App. A).

We note in passing that the above described approach also resembles the multilevel blocking strategy [30]: On the first level, the harmonic bath degrees of freedom are integrated out, while on the second level the quasi-classical coordinates get eliminated; the addend in Eq. (38) then corresponds to the respective level-2 bonds. It furthermore seems noteworthy that, while here we only present results for electronic systems with constant nearest-neighbor coupling, $\Delta_{s,s'} = \delta_{s'-s,1}\Delta$, the above outlined approach is suitable for arbitrary electronic systems as long as they can be described by a finite Hilbert space. Corresponding applications will be shown in a subsequent paper.

V. NUMERICAL RESULTS

Next we present results for a symmetric donor-bridge-acceptor (DBA) system (degenerate donor and acceptor energies, degenerate bridge states with energy gap $\hbar\epsilon$ between bridge and donor/acceptor) with constant nearest neighbor coupling obtained from PIMC simulations as

described above. Albeit its simplicity this model captures essential features of bridge mediated ET and can serve as a basis for more elaborate studies. In part, this work was motivated by former theoretical approaches on symmetric DBA systems [4, 8, 9] which, however, relied on simpler system+reservoir models and/or approximate numerical methods. In particular, in contrast to these latter, the formulation (7) takes the dynamics of the vibronic structure of the DBA compound fully into account. Further, the MC approach is not plagued by the limitations of Redfield theory, but rather applies also to low temperatures, slower bath modes, and stronger dissipation. Hence, it reproduces in the proper limits the known analytical findings specified in Sec. III B.

Clearly, the ET process considered here eventually leads to thermal equilibration of the electronic sites. Due to the relation between relaxation rates and conductances in stationary non-equilibrium [14], our results give also insight, at least qualitatively, into ET through metal-molecule-metal junctions. In fact, to get quantitative results, the present approach can in principle be extended to the latter case by eliminating the electronic states in the metal contacts as an additional bath. Corresponding work is in progress.

The superexchange mechanism is a truly quantum mechanical coherence phenomenon. Thus, in order to investigate this scenario in more detail within the MC approach, we choose parameters such that for lower temperatures the population dynamics exhibits coherent oscillations, while for slightly higher T, with a bath that is still quantum mechanically, a rate description is applicable. We take a damping coefficient $\alpha = 1/4$ well below the coherent-incoherent transition $\alpha = 1/2$ [18] and a moderate cut-off frequency $\omega_c/\Delta = 5$ so that adiabatic effects are expected to show up. Note that the cutoff frequency ω_c also defines the maximum of the spectral density distribution (35), such that even frequencies somewhat larger than ω_c contribute. The classical reorganization energy follows as $\Lambda_{\rm cl} = 2\alpha\omega_c = 2.5\Delta$. Accordingly, we expect superexchange, if important, to be particularly pronounced.

To confirm the proper choice of the above parameters and to fix the temperature range where a description in terms of rate constants applies, we start by presenting results for the equilibrium bridge population P_B^∞ of a three-state system at a fixed bridge energy $\epsilon/\Delta = 5$ for varying temperature. As can be seen by comparing P_B^∞ obtained from imaginary-time MC simulations with a simple Boltzmann distribution, i.e. $1/[2\exp(\beta\epsilon)+1]$, deviations occur for $\hbar\beta\Delta > 0.3$ related to the strong influence of quantum delocalization (see Fig. 2). This triggers the tendency of coherent oscillations in the population dynamics which becomes especially obvious for an energetically degenerated bridge (see Fig. 3). Damped oscillations are clearly observable in the intermediate state for $\hbar\beta\Delta > 0.3$. These results verify that (i) with the above choice of parameters electronic coherent effects are crucial and (ii) that the ET dynamics can be captured by
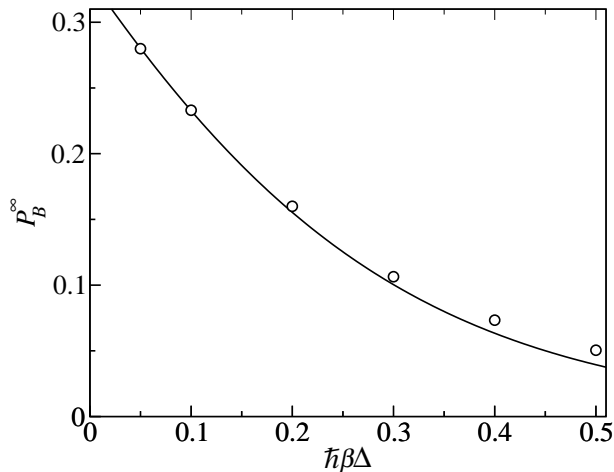
FIG. 2: Equilibrium occupation probabilities P_B^∞ of the bridge state for $S = 1$, $\epsilon/\Delta = 5$, $\alpha = 1/4$ and $\omega_c/\Delta = 5$ as a function of inverse temperature. Circles denote imaginary-time QMC results (with error bars smaller than symbol size) while the solid line refers to $1/[2e^{\hbar\beta\epsilon}+1]$ according to a Boltzmann distribution.

transfer rates for $\hbar\beta\Delta < 0.3$. With respect to the bath, a typical temperature $\hbar\beta\Delta = 0.1$ corresponds at the maximum $\omega_{max} = \omega_c$ of the spectral density to $\hbar\beta\omega_{max} = 0.5$ so that a high temperature approximation does not apply. The simulations have been performed for system times long enough and sufficient stochastical accuracy to allow for studying details of the dynamics even close to the approach of equilibrium.

Having fixed the proper range of parameters, we now turn to a detailed analysis of the population dynamics. First, we consider a three-state system with varying bridge energy $0 \leq \epsilon/\Delta \leq 20$ and at a fixed temperature $\hbar\beta\Delta = 0.1$ (Fig. 4). For bridges with $\epsilon/\Delta \leq 7.5$ the intermediate state approaches thermal equilibrium within the simulation period. Interestingly, a bridge energy $\epsilon/\Delta = 2.5$ leads to an increase of the acceptor population almost as fast as for the degenerate case $\epsilon/\Delta = 0$. This is due to the fact that for the former bridge the equilibrium population P_A^∞ is larger while the bridge is still not high enough to considerably reduce the donor-bridge rate Γ_{DB}. The population dynamics for this system can now be analyzed with the full (17) and the sequential (18) model to extract the rate constants for times $t > t_{trans}$. The rate constants were then obtained by repeating this procedure for successively increasing t_{trans} such that the corresponding rates eventually saturate at plateau values. The latter are depicted in Fig. 5 where also the nonadiabatic classical Marcus (21) and the golden rule (22) results are shown. The numerical results basically follow the latter ones with minor deviations that can be attributed to adiabatic effects (e.g. recrossing phenomena) not included in the golden rule rate expression. Sequential rates are extracted for all three electronic states where those obtained from the donor and acceptor coincide while rates extracted from the bridge exceed the
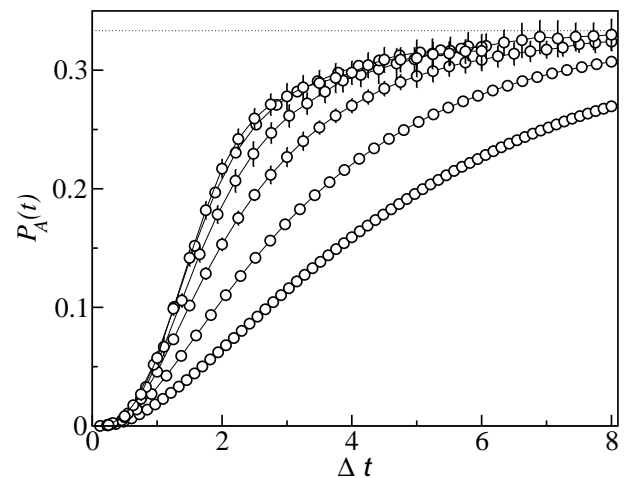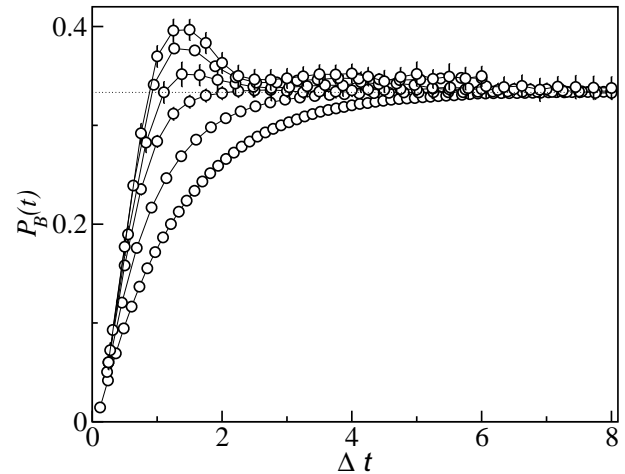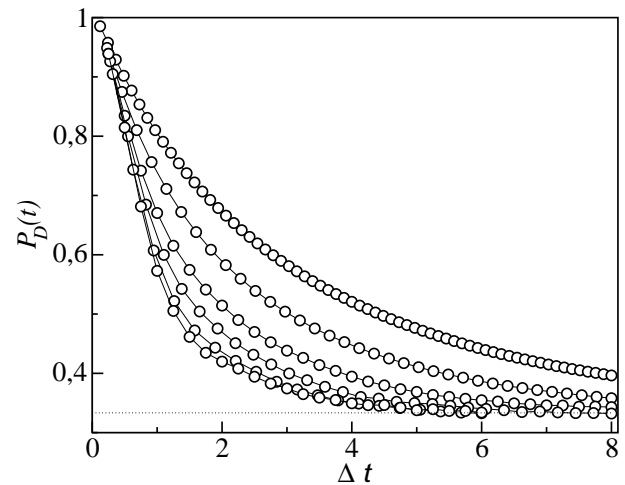

FIG. 3: Donor, bridge, and acceptor populations $P_D(t)$, $P_B(t)$, and $P_A(t)$, respectively (from top to bottom), for $S = 1$, $\epsilon/\Delta = 0$, $\alpha = 1/4$, $\omega_c/\Delta = 5$, and (top to bottom for donor, bottom to top for bridge and acceptor) $\hbar\beta\Delta = 0.05, 0.1, 0.2, 0.3, 0.4$, and 0.5. Error bars correspond to one standard deviation in each direction. Dotted lines denote the equilibrium population $P_D^\infty = P_B^\infty = P_A^\infty = 1/3$. The solid lines are guides for the eye only.
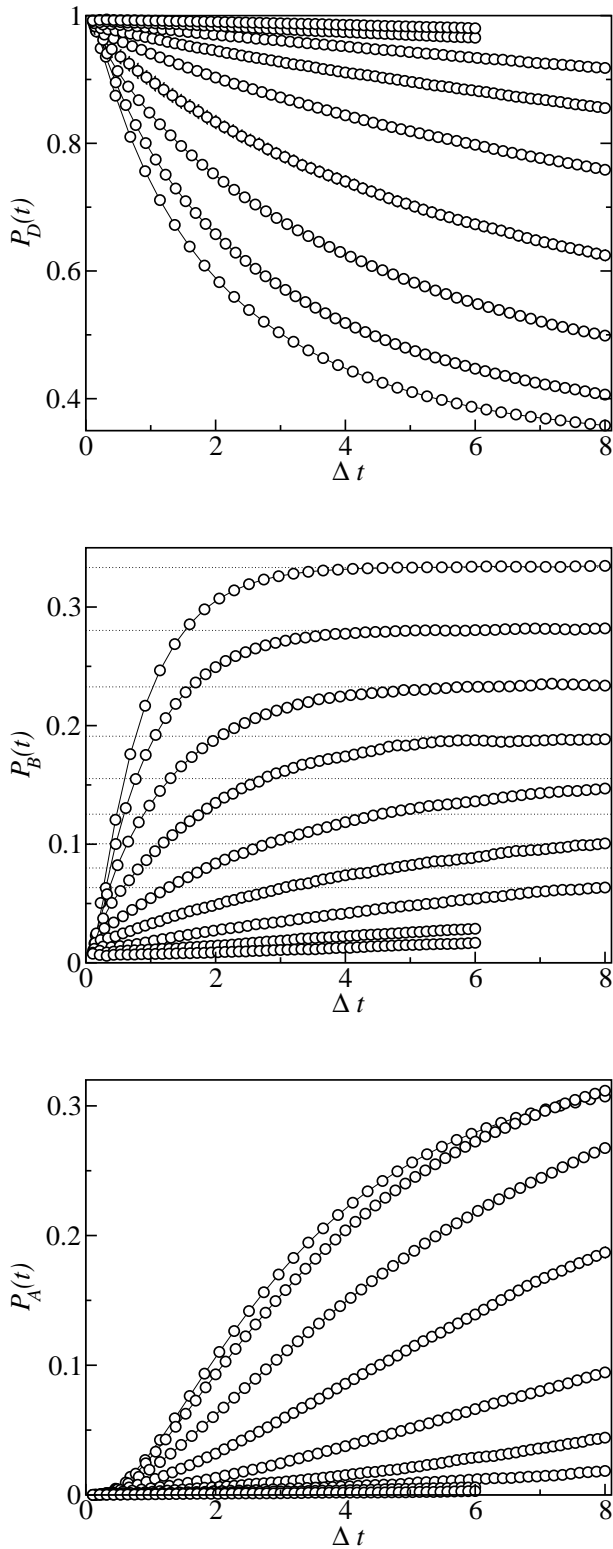
FIG. 4: Donor, bridge, and acceptor populations $P_D(t)$, $P_B(t)$, and $P_A(t)$, respectively (from top to bottom), for $S = 1$, $\alpha = 1/4$, $\omega_c/\Delta = 5$, $\hbar\beta\Delta = 0.1$, and (top to bottom for bridge and acceptor, bottom to top for donor) $\epsilon/\Delta = 0$, 2.5, 5, 7.5, 10, 12.5, 15, 17.5, and 20. Error bars correspond to one standard deviation in each direction. Dotted lines denote the respective Boltzmann equilibrium populations of the bridge state. The solid lines are guides for the eye only.
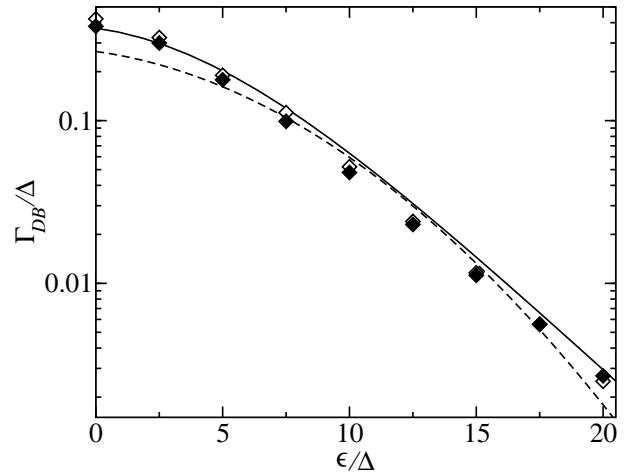

FIG. 5: Sequential transfer rates Γ_{DB} obtained from the bridge state (open diamonds) and donor and acceptor state (closed diamonds) for $S = 1$, $\alpha = 1/4$, $\omega_c/\Delta = 5$, and $\hbar\beta\Delta = 0.1$ as a function of ϵ. The solid line refers to the golden rule rate (22), the dashed one to the Marcus rate (21).

former by about 5-10%. This deviation signals a short-coming of Eqs. (18) and (19) in this parameter regime. In fact, the reduction of Eq. (16) to Eq. (17) is in a strict sense only justified in the strongly damped regime. The impact of superexchange, however, is very weak and its corresponding rates are smaller by two orders of magnitude. Accordingly, the sequence of superexchange rates for various t_{trans} obtained from the fitting procedure described above does not saturate but rather strongly fluctuates such that a quantitative description is out of range.

This behavior can be understood from the analytical rate expressions. Namely, upon closer inspection of Eqs. (24) and (21) one derives that in the *classical regime* $\Gamma_{SCL,\text{GR}}$ dominates against the sequential transfer $\Gamma_{DB,\text{Marcus}}$ whenever $\hbar\beta\epsilon \gg 1$ and $\epsilon \gg \Lambda_{\text{cl}}$ such that

$$\frac{\Gamma_{SCL,\text{GR}}}{\Gamma_{DB,\text{Marcus}}} \approx \frac{\Delta^2}{\epsilon^2} \exp(\beta\hbar\epsilon^2/4\Lambda_{\text{cl}}) \gg 1 . \qquad (39)$$

This verifies the expected and well-known fact that for a classical bath the superexchange mechanism prevails whenever thermal activation from D to B is suppressed. For a *quantum bath*, however, the situation is more restrictive. From Eq. (23) one estimates $\Gamma_{SQM,\text{GR}} \propto \Delta^4/(\omega_c\epsilon^2)$ for $\hbar\beta\omega_c > 1$ (and α of order 1) such that for fixed temperature $\hbar\beta\Delta < 0.5$ superexchange transport prevails only for extremely high bridge energies, i.e. $\epsilon/\Delta > 40$, where the transfer is essentially frozen on the time scale accessible in MC simulations and in realistic experiments. With electronic couplings of the order of $100\,\text{cm}^{-1}$ [4, 8], the above condition requires at $T \simeq 150\,\text{K}$ bridge energies of the order of $\epsilon \approx 5000\,\text{cm}^{-1}$ leading to typical transfer times of the order of $30\,\mu\text{s}$. Having in mind that our primary focus is to identify regions where one of the transfer channels, sequential or superexchange, *dominates*, superexchange turns out to

be negligible in Fig. 4.

At least as a minor effect we find superexchange in the ET dynamics shown in Fig. 4 for $\epsilon/\Delta \geq 5$. We thus performed simulations for fixed bridge energy, but varying temperature $0.05 \leq \hbar\beta\Delta \leq 0.5$, see Fig. 6. As already mentioned, for $\hbar\beta\Delta > 0.3$ a rate description is questionable as the bridge population shows signs of coherent oscillations. Sequential rates are extracted according to the above scheme from donor and acceptor as well (cf. Fig. 7). The results are in qualitative agreement with the golden rule description with deviations between donor and acceptor rates appearing in the low temperature range where quantum coherences exist. All numerical rates are below the nonadiabtic values, again due to adiabatic effects in the bath dynamics. Superexchange cannot be found. This is understood from the above discussion: For fixed ϵ the analytical superexchange rate exceeds the golden rule one only in the temperature range $\hbar\beta\Delta \gg 2\ln(\epsilon/\Delta)/(\epsilon/\Delta)$ corresponding to low temperatures $\hbar\beta\Delta \gg 0.6$ where, as seen above, for weaker dissipation ($\alpha < 1/2$) a rate description is in a strict sense no longer feasible. The situation changes when donor and acceptor are biased with an energy gap $\epsilon_{DA} = \epsilon_D - \epsilon_A > 0$. Then, based on the generalization of Eq. (23) for $\epsilon_{DA} \neq 0$ [33] one can show for a high lying intermediate state that superexchange exceeds sequential transport already at higher temperatures $\hbar\beta\Delta \gg 2\ln(\epsilon/\Delta)/[(\epsilon_{DA}+\epsilon)/\Delta]$. In fact, for biased ET systems indications of superexchange have already been seen in previous MC simulations for three-state systems [26].

Let us now turn to longer bridges with $b = d - 2 > 1$. The stability of the MC procedure allows to extract rate constants for systems up to $b = 10$. In Fig. 8 results for $b = 1$ up to $b = 10$ bridge states are displayed. Apparently, the donor dynamics basically saturates for $b > 2$ on the time scale of the simulations meaning that the donor decay depends on the bridge length only at very large times and then only slightly. This amounts to the fact that the equilibrium populations decrease only algebraically with b. In contrast, the time evolution of the acceptor and its closest bridge states are strongly affected by the varying bridge length. The numerical data can be very precisely reproduced by a sequential transfer model according to Eq. (18) where due to symmetry and detailed balance only two fit parameters enter, namely the forward rate from the donor Γ_{DB} and the bridge rate Γ_B. It turns out that by fixing these parameters at $\Gamma_{DB} = 0.284$ and $\Gamma_B = 0.348$ *all* populations independent of the bridge length can be described, thus verifying that the transport is more or less completely sequential. The nonadiabatic golden rule formula (22) predicts a little bit higher values $\Gamma_{DB,GR} = 0.297$ and $\Gamma_{B,GR} = 0.37$ in agreement with our findings for the three-state system. Our main focus lies on the behavior of the smallest eigenvalue of the rate matrix A, i.e. the relaxation rate Γ_R, as the bridge length b increases. Since an analytical diagonalization of A for arbitrary b is not
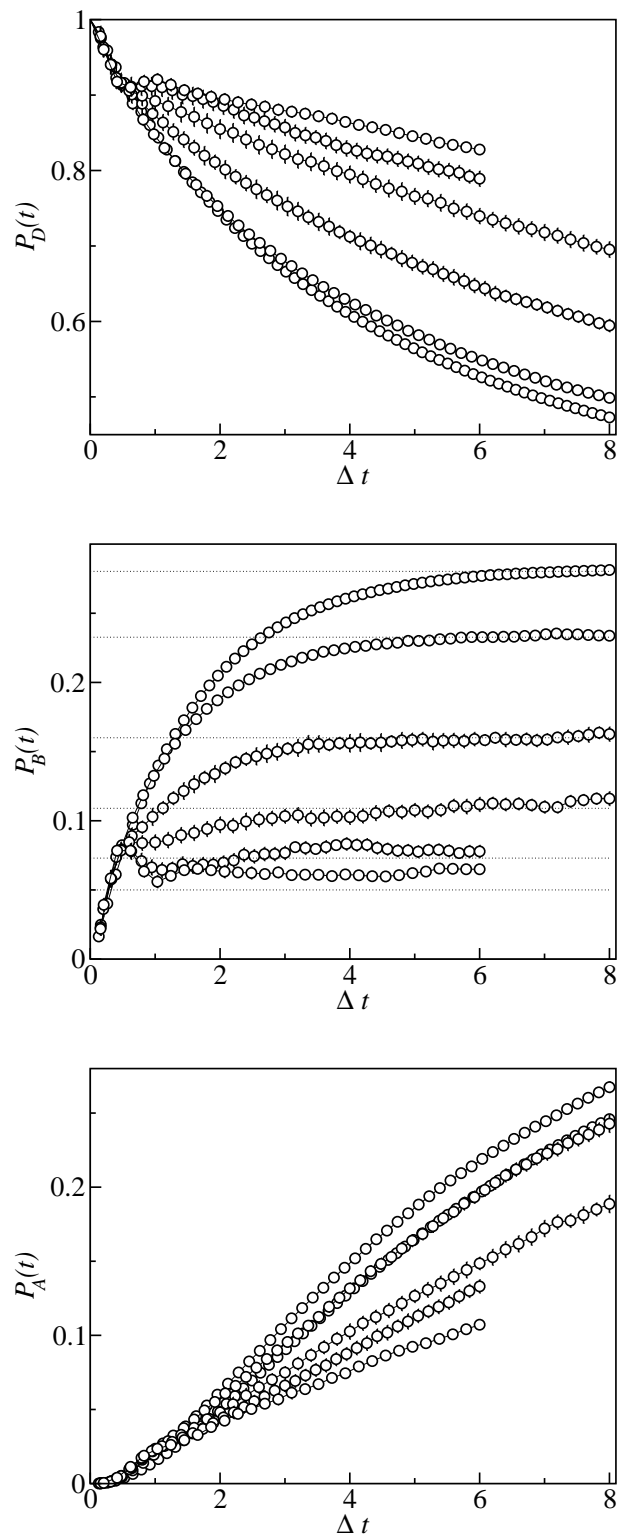

FIG. 6: Donor, bridge, and acceptor populations $P_D(t)$, $P_B(t)$, and $P_A(t)$, respectively (from top to bottom), for $S = 1$, $\epsilon/\Delta = 5$, $\alpha = 1/4$, $\omega_c/\Delta = 5$, and (top to bottom for bridge and acceptor, bottom to top for donor) $\hbar\beta\Delta = 0.05, 0.1, 0.2, 0.3, 0.4,$ and 0.5. Error bars correspond to one standard deviation in each direction. Dotted lines denote the respective equilibrium populations from Fig. 2 of the bridge state. The solid lines are guides for the eye only.
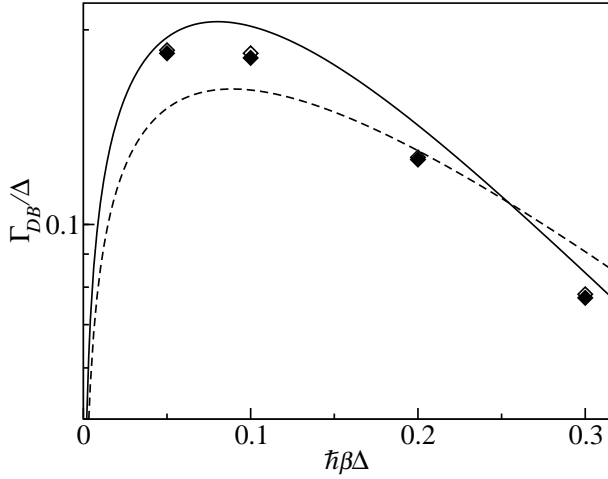
FIG. 7: Sequential transfer rates Γ_{DB} obtained from the bridge state (open diamonds) and donor and acceptor state (closed diamonds) for $S = 1$, $\epsilon/\Delta = 5$, $\alpha = 1/4$, and $\omega_c/\Delta = 5$ as a function of inverse temperature. The solid line refers to the golden rule rate (22), the dashed one to the Marcus rate (21).

possible, we invoke an effective DBA model to capture the key features and compare with the numerical results. Accordingly, we follow Ref. [9] and consider in addition to the donor and the acceptor population only the bridge populations P_{BD} and P_{BA} coming from the donor and acceptor, respectively. The dynamics of these populations $\mathcal{P} = (P_D, P_{BD}, P_{BA}, P_A)$ is then determined by $\dot{\mathcal{P}} = \mathcal{A}\mathcal{P}$ with the reduced rate matrix

$$\mathcal{A} = \begin{pmatrix} -\Gamma_{DB} & \Gamma_r & \Gamma_d & 0 \\ \Gamma_{DB} & -\Gamma_r - \Gamma_d & 0 & 0 \\ 0 & 0 & -\Gamma_r - \Gamma_d & \Gamma_{DB} \\ 0 & \Gamma_d & \Gamma_r & -\Gamma_{DB} \end{pmatrix} . \quad (40)$$

Here, Γ_r denotes the recrossing rate from the bridge back to donor/acceptor and Γ_d the rate for the diffusive motion from one end to the other end of the bridge. The smallest eigenvalue can now be found analytically and reads

$$\Gamma_R = \frac{\Gamma_{DB}}{2} \left[1 + \mu_r + \mu_d - \sqrt{(1 + \mu_r + \mu_d)^2 - 8\mu_d} \right]$$
$$(41)$$

where for convenience we introduced $\mu_{r/d} = \Gamma_{r/d}/\Gamma_{DB}$. In Ref. [9] it was found that $\mu_r/\mu_d = b$. Since Γ_{DB} is independent of the bridge length, the ratio μ_d can be inferred from the mean first passage time of a particle diffusing across a one-dimensional wire [37]. This scales like b^2 so that $\mu_d = 1/(\nu b^2)$ where ν is a constant. Based on these results two scenarios for $\Gamma_R(b)$ can be distinguished. For short and moderate long bridges with b sufficiently smaller than $1/\nu$ ($\mu_d > 1$), Eq. (40) gives rise to $\Gamma(b) \approx \Gamma_{DB} \, 2/(1+b)$, while for longer bridges $b \gg 1/\nu$ ($\mu_d \ll 1$) the approximation $\Gamma_R(b) \approx \Gamma_{DB} \, 2/(\nu b^2)$ applies. In the first case the bottleneck of the transfer process is the donor-bridge activation encoded in Γ_{DB}, in
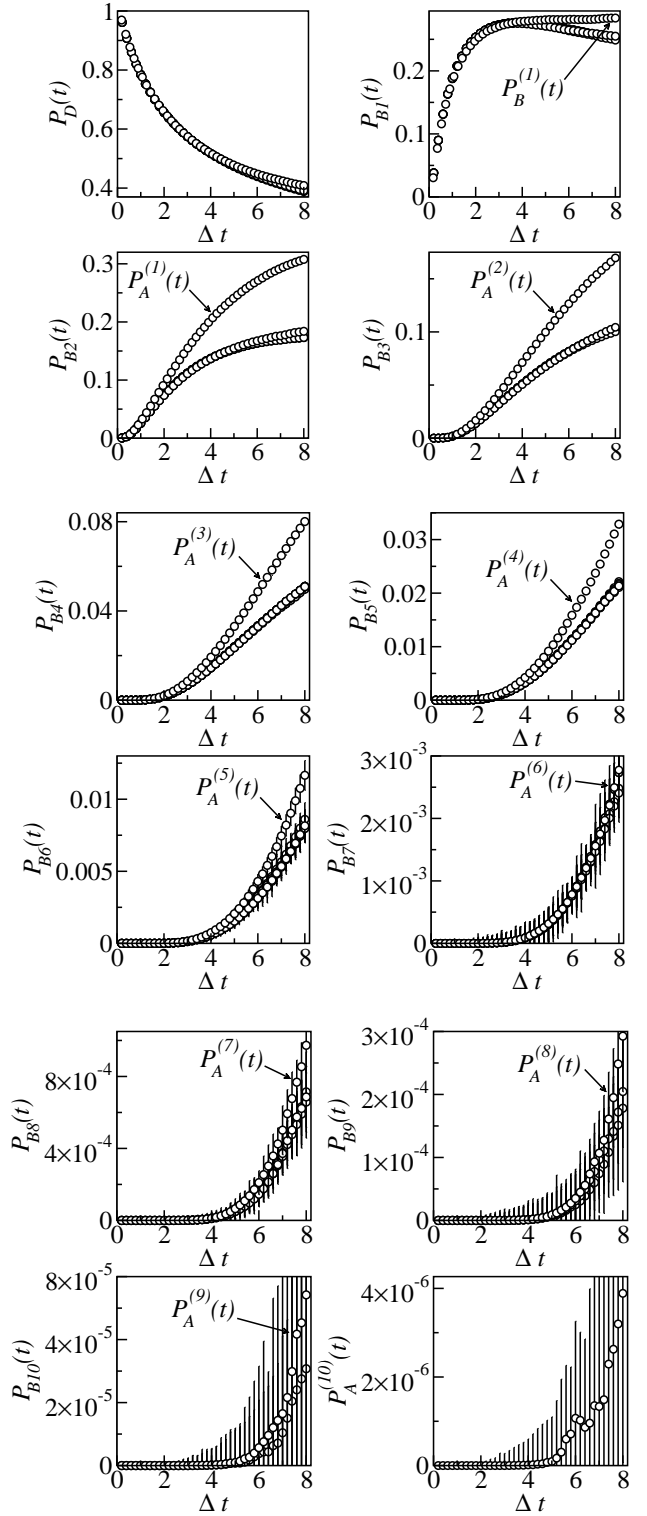

FIG. 8: Electronic populations for $\epsilon/\Delta = 2.5$, $\alpha = 1/4$, $\omega_c/\Delta = 5$, $\hbar\beta\Delta = 0.1$, and $1 \leq S \leq 3^1/_2$ ($b = 1, \ldots, 10$). $P_A^{(b)}$ denotes the acceptor population for a system with b bridge states.
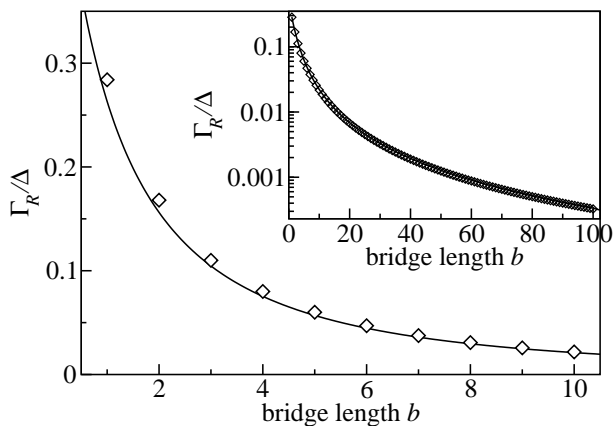
FIG. 9: Relaxation rate Γ_R for $\epsilon/\Delta = 2.5$, $\alpha = 1/4$, $\omega_c/\Delta = 5$, $\hbar\beta\Delta = 0.1$, and $1 \leq S \leq 3^{1/2}$ ($1 \leq b \leq 10$) (open diamonds). The solid line resembles Eq. (42). The rates in the inset correspond to the golden rule rate (22).

the latter one the rate is limited by the diffusive motion along the entire bridge described by Γ_d. An effective formula comprising these limiting cases is given by

$$\Gamma_R(b) \approx \Gamma_{DB} \frac{2}{1 + b + \nu b^2} . \tag{42}$$

Indeed, the numerical data shown in Fig. 9 are quantitatively captured by the result (42) with $\nu = 0.159$. Due to this excellent agreement between sequential transfer model and the PIMC data on the one hand and between the corresponding relaxation rates and the expression (40) on the other hand, we extracted the relaxation rate from the full rate matrix A for bridges with up to $b = 100$ and confirmed the validity of Eq. (40).

A functional behavior of the form $\Gamma_R(b) \propto 1/b$ has been noted empirically already in Ref. [8], derived theoretically in Ref. [9] (in a slightly different model though), and observed experimentally in a variety of molecular systems [7, 11, 14]. In lead-molecule-lead junctions it gives rise to Ohm's law in the current voltage characteristics. Our above findings indicate that, at least in symmetric DBA systems, this behavior is characteristic for situations where Γ_{DB} is sufficiently smaller than the bridge diffusion rate. However, a changeover to $\Gamma(b) \propto 1/b^2$ should be observable for very long bridges.

VI. CONCLUSIONS

Electron transfer processes across molecular chains have gained much interest in recent years, particularly in the context of molecular electronics. Motivated by previous studies, in this paper the electronic dynamics across symmetric donor-bridge-acceptor systems has been analyzed based on a numerically exact treatment of the corresponding dissipative quantum system within a real-time MC scheme.

Upon improving existing filter techniques we have been able to achieve accurate data for the population dynamics even for times where equilibration sets in or has already been established, and for an increasing number of electronic bridge states. This opens the door to consider a variety of electronic site topologies as well as the impact of external time dependent fields. Eventually, by a proper reduction of the Hilbert space also the reduced dynamics of continuous degrees of freedom with a discrete energy spectrum of the bare system are now accessible. Corresponding work in this direction is in progress.

Physically, the main issue has been the role of superexchange and sequential transport in symmetric DBA compounds. Here, results based on Redfield theory and simplified system-bath couplings indicated different regimes for the length dependence of net transfer across the bridge comprising an exponential and an algebraic falloff, respectively. The numerical MC data have been analyzed by exploiting the fact that (i) the ET dynamics can in the range of parameters considered be mapped onto Master equations with time independent transition rates and (ii) the path integral formulation reproduces the known analytical findings for these rates in certain limits. For the DBA compound the parameters were chosen to guarantee strong quantum effects, i.e. moderate dissipation, sufficiently low temperatures, and a broad distribution of bath modes.

The conclusion of the numerical results together with the analytical findings is that in a symmetric DBA system (degenerate donor and acceptor energy) even for weaker dissipation superexchange can be expected to dominate only for classical or nearly classical bath. For quantum mechanical baths as they have been studied here, it does not play a significant role for ET processes that can be captured by time independent transport rates. Particularly, in contrast to earlier studies we found no dominant role of the superexchange mechanism neither for relatively high lying bridges, nor for lower temperatures or more bridge sites. For quantum baths it requires extremely high lying bridge states with essentially frozen dynamics or temperatures that are so low that coherences give rise to oscillating population dynamics associated with a breakdown of a conventional rate description. Experimentally, a clear observation of a changeover from tunneling to hopping dominated transfer in molecular chains has not been found yet, a fact, that may to some extent be attributed to the scenario we have revealed. The results reported in Ref. [7] show some indications but not a direct proof though, since the energetic landscape of the molecular structures changes with their length. By varying the number of bridge sites an algebraic decrease of the relaxation rate could be confirmed for shorter as well as longer bridges. Based on a reduced DBA model we find a changeover from a range where the donor-bridge activation limits the transfer to a domain where the nondirectional diffusive motion along the wire is decisive. Previous simulations on biased three-state systems suggest in accordance with the analytical

results that an energy gap between donor and acceptor (in addition to the energy gap between the bridge and donor/acceptor) stimulates the occurrence of superexchange.

APPENDIX A: COMPUTATIONAL DETAILS

For the sake of computational savings, we calculate

$$P_{s_f,s_i}(t_k) = \frac{1}{2} \sum_{\{s_j\}} \left(\delta_{s_k,s_f} + \delta_{s'_k,s_f} \right) \delta_{s_1,s_i} \rho[\{s_j\}] ,$$
$$k = 1, \ldots, q+1 \qquad (A1)$$

rather than Eq. (26), such that one single MC trajectory can be used to compute P_{s_f,s_i} for all times $t_k = (k-1)\tau$, where the simultaneous measurement on the forward and backward path enhances the statistics. Equation (38) then becomes

$$P_{s_f,s_i}(t) = \frac{1}{2} \sum_{\{\xi_j\},\eta_{q+1}} \exp\left[-\sum_{j=2}^{q} \xi_j \left(i\hat{X}_j^{(s_i)} \right. \right.$$
$$\left. \left. + \sum_{k \geq j} \xi_k \Lambda_{k-j} \right) \right] \hat{K}^{(1)}(\xi_2, \ldots, \xi_q) \cdots$$
$$\times \bar{K}^{(j;s_f)}(\xi_j, \ldots, \xi_q) \cdots \hat{k}^{(q)}(\xi_q, \eta_{q+1}) , \qquad (A2)$$

where $\bar{K}^{(j;s_f)}(\xi_k, \ldots, \xi_q)$ is defined by

$$\bar{K}_{\eta_j,\eta_{j+1}}^{(j;s_f)}(\xi_j, \ldots, \xi_q) = \frac{1}{2} \left(\delta_{\eta_k+\xi_k,2s_f} + \delta_{\eta_k-\xi_k,2s_f} \right)$$
$$\times \hat{K}_{\eta_j,\eta_{j+1}}^{(j)}(\xi_j, \ldots, \xi_q) \qquad (A3)$$

and $\hat{K}^{(1)}$ again is a row vector due to $\eta_1 \equiv 2s_i$, while $\hat{k}^{(q)}(\xi_q, \eta_{q+1})$ denotes the η_{q+1}'s column of $\hat{K}^{(q)}(\xi_q)$.

Another significant reduction of the computational costs of the MC calculations can be obtained by optimizing the MC weight. While

$$w_{\mathrm{MC}}(\{\xi_j\}, \eta_{q+1}) \equiv \exp\left(-\sum_{k \geq j=2}^{q} \xi_k \Lambda_{k-j} \xi_j \right)$$
$$\times \left| \hat{K}^{(1)}(\xi_2, \ldots, \xi_q) \cdots \hat{k}^{(q)}(\xi_q, \eta_{q+1}) \right| \qquad (A4)$$

generally represents a natural choice for the MC weight, for systems with sufficiently weak damping an attractive

alternative is given by

$$\tilde{w}_{\mathrm{MC}}(\{\xi_j\}, \eta_{q+1}) \equiv \left| \tilde{K}^{(1)}(0, \xi_2) \cdots \tilde{k}^{(q)}(\xi_q) \right| \qquad (A5)$$

with the real-valued matrices

$$\tilde{K}_{\eta,\eta'}(\xi, \xi') = |\langle(\eta+\xi)/2| \exp(-i\tau H_{d\mathrm{LS}}/\hbar)|(\eta'+\xi')/2\rangle| , \qquad (A6)$$

which essentially neglect all dissipative effects. Although MC runs utilizing $\tilde{w}_{\mathrm{MC}}$ exhibit somewhat poorer statistics than those using w_{MC}, the switching from complex to real-valued matrices which furthermore, unlike the $\hat{K}^{(j)}$, can be calculated and stored before executing the MC moves results in a significant speedup of the simulations. In fact, for the parameters investigated here, using Eq. (A5) over (A4) could reduce the computational costs by a factor of roughly four. Note that the restriction of the use of $\tilde{w}_{\mathrm{MC}}$ to the weakly damped regime does not really impose a severe limitation since for sufficiently strong dissipation the overall sign problem will be weak enough to be tackled by any conventional PIMC scheme.

APPENDIX B: POPULATION DYNAMICS FOR $S = 1$

For $S = 1$, explicit and transparent expressions for the electronic populations can be gained from Eq. (18) and (19). Allowing some transient motion for times $t < t_{\mathrm{trans}}$, one easily obtains

$$P_D(t_{\mathrm{trans}} + t) =$$
$$\frac{1}{2}\left\{ 1 + [P_D(t_{\mathrm{trans}}) - P_A(t_{\mathrm{trans}})]e^{-(\Gamma_{DB}+\Gamma_S)t} \right.$$
$$- [P_B^\infty - P_B(t_{\mathrm{trans}})] \left[1 - \exp\left(-\frac{\Gamma_{DB}}{P_B^\infty}t \right) \right]$$
$$\left. - P_B(t_{\mathrm{trans}}) \right\} ,$$

$$P_B(t_{\mathrm{trans}} + t) =$$
$$[P_B^\infty - P_B(t_{\mathrm{trans}})] \left[1 - \exp\left(-\frac{\Gamma_{DB}}{P_B^\infty}t \right) \right]$$
$$+ P_B(t_{\mathrm{trans}}) ,$$

$$P_A(t_{\mathrm{trans}} + t) =$$
$$\frac{1}{2}\left\{ 1 + [P_A(t_{\mathrm{trans}}) - P_D(t_{\mathrm{trans}})]e^{-(\Gamma_{DB}+\Gamma_S)t} \right.$$
$$- [P_B^\infty - P_B(t_{\mathrm{trans}})] \left[1 - \exp\left(-\frac{\Gamma_{DB}}{P_B^\infty}t \right) \right]$$
$$\left. - P_B(t_{\mathrm{trans}}) \right\} , \qquad (B1)$$

[1] J. Jortner and M. Bixon, eds., Adv. Chem. Phys. **106**, 107 (1999).

[2] R.A. Marcus, J. Chem. Phys. **24**, 966 (1956).

[3] R.A. Marcus and N. Sutin, Biochim. Biophys. Acta **811**, 265 (1985).

[4] A.K. Felts, W.T. Pollard, and R.A. Friesner, J. Phys. Chem. **99**, 2929 (1995).

[5] A. Okada, V. Chernyak, and S. Mukamel, J. Phys. Chem. A **102**, 1241 (1997).

[6] W.B. Davis, M.R. Wasielewski, M. Ratner, V. Mujica, and A. Nitzan, J. Phys. Chem. **101**, 6158(1997).

[7] W.B. Davis, W.A. Svec, M.A. Ratner, and M.R. Wasielewski, Nature **396**, 60 (1998).

[8] D. Segal, A.Nitzan, W.B. Davis, M.R. Wasielewski, and M.A. Ratner, J. Phys. Chem. **104**, 3817 (2000).

[9] E. Hershkovitz and E. Pollak, Ann. Phys. (Leipzig) **9**, 764 (2000).

[10] C. Dekker and M.A. Ratner, Phys. World **14**, 29 (2001).

[11] M. Magoga and C. Joachim, Phys. Rev. B **56**, 4722 (1997).

[12] J. Jortner and M.A. Ratner (eds.), *Molecular Electronics*, (Blackwell Sci., Oxford, 1997).

[13] C. Kergueris, J.-P. Bourgoin, S. Palacin, D. Esteve, C. Urbina, M. Magoga, and C. Joachim, Phys. Rev. B **59**, 12505 (1999).

[14] A. Nitzan, Ann. Rev. Phys. Chem. **52**, 681 (2001).

[15] P. Hänggi and M.A. Ratner (eds.), Chem. Phys. **281**, (2002).

[16] D. Chandler, in *Liquids, Freezing and the Glass Transition*, ed. by D. Levesque, J.P. Hansen. and J. Zinn-Justin (Elsevier Science, North Holland, 1991), Les Houches 51, Part 1.

[17] X. Song and A.A. Stuchebrukhov, J. Chem. Phys. **99**, 969 (1993).

[18] U. Weiss, *Quantum Dissipative Systems*, Series in Modern Condensed Matter Physics, Vol. 2 (World Scientific, Singapore, 1998).

[19] R.P. Feynman and F.L. Vernon, Ann. Phys. (N.Y.) **24**, 118 (1963).

[20] A.O. Caldeira and A.J. Leggett, Ann. Phys. (NY) **149**, 374 (1983); *ibid.* **153**, 445(E) (1983).

[21] N. Makri and D.E. Makarov, J. Chem. Phys. **102**, 4600 (1995).

[22] *Quantum Monte Carlo Methods in Condensed Matter Physics*, ed. by M. Suzuki (World Scientific, Singapore, 1993), and references therein.

[23] A. Lucke, C.H. Mak, R. Egger, J. Ankerhold, J.T. Stockburger, and H. Grabert, J. Chem. Phys. **118**, 291 (1997).

[24] A. Lucke and J. Ankerhold, J. Chem. Phys. **115**, 4696 (2001).

[25] L. Mühlbacher and R. Egger, J. Chem. Phys. **118**, 179 (2003).

[26] R. Egger and C.H. Mak, Phys. Rev. B **50**, 15210 (1994); R. Egger and C.H. Mak, J. Phys. Chem. **98**, 9903 (1994).

[27] S. Chakravarty and J. Rudnick, Phys. Rev. Lett. **75**, 501 (1995).

[28] V.S. Filinov, Nucl. Phys. B **271**, 717 (1986).

[29] See, for example, J.D. Doll and D.L. Freeman, in *Lasers, Molecules, and Methods*, ed. by J.O. Hirschfelder, R.E. Wyatt, and R.D. Coalson, Adv. Chem. Phys. Vol. LXXIII (Wiley, New York, 1989).

[30] C.H. Mak and R. Egger, Adv. Chem. Phys. **93**,39 (1996).

[31] C.H. Mak, R. Egger, and H. Weber-Gottschick, Phys. Rev. Lett. **81**, 4533 (1998); R. Egger, L. Mühlbacher, and C.H. Mak, Phys. Rev. E **61**, 5961 (2000).

[32] R. Egger, C.H. Mak, and U. Weiss, J. Chem. Phys. **100**, 2651 (1994).

[33] R. Egger, C.H. Mak, and U. Weiss, Phys. Rev. E **50**, (655)(R) (1994).

[34] H. Grabert, U. Weiss, and P. Talkner, Z. Phys. B **55**, 87 (1984).

[35] J. Ankerhold and H. Lehle, J. Chem. Phys. **120**, 1436 (2004).

[36] J. Reichert, R. Ochs, H.B. Weber, M. Mayor and, H.v. Löhneysen, Appl. Phys. Lett. **82**, 4137 (2003).

[37] R. Landauer and M. Büttiker, Phys. Rev. B **36**, 6255 (1987).